

Submitted to the Astrophysical Journal

The expanding bipolar shell of the helium nova V445 Puppis

P. A. Woudt

*Department of Astronomy, University of Cape Town, Private Bag X3, Rondebosch 7701,
South Africa*

Patrick.Woudt@uct.ac.za

D. Steeghs¹

Department of Physics, University of Warwick, Coventry, CV4 7AL, United Kingdom

M. Karovska

*Harvard-Smithsonian Center for Astrophysics, 60 Garden Street, Cambridge MA
02138-1516, USA*

B. Warner²

*Department of Astronomy, University of Cape Town, Private Bag X3, Rondebosch 7701,
South Africa*

P. J. Groot and G. Nelemans

*Department of Astrophysics, Radboud University Nijmegen, PO Box 9010, 6500 GL,
Nijmegen, the Netherlands*

G. H. A. Roelofs

*Harvard-Smithsonian Center for Astrophysics, 60 Garden Street, Cambridge MA
02138-1516, USA*

T. R. Marsh

Department of Physics, University of Warwick, Coventry, CV4 7AL, United Kingdom

T. Nagayama

*Department of Astronomy, Kyoto University, Kitashirakawa-Oiwake-cho, Sakyo-ku, Kyoto
606-8502, Japan*

D. P. Smits

*Department of Mathematical Sciences, University of South Africa, UNISA, Pretoria 0003,
South Africa*

and

T. O’Brien

*University of Manchester, Jodrell Bank Observatory, Macclesfield, Cheshire SK11 9DL,
United Kingdom*

ABSTRACT

From multi-epoch adaptive optics imaging and integral field unit spectroscopy we report the discovery of an expanding and narrowly confined bipolar shell surrounding the helium nova V445 Puppis (Nova Puppis 2000). An equatorial dust disc obscures the nova remnant, and the outflow is characterised by a large polar outflow velocity of $6720 \pm 650 \text{ km s}^{-1}$ and knots moving at even larger velocities of $8450 \pm 570 \text{ km s}^{-1}$. We derive an expansion parallax distance of $8.2 \pm 0.5 \text{ kpc}$ and deduce a pre-outburst luminosity of the underlying binary of $\log L/L_{\odot} = 4.34 \pm 0.36$. The derived luminosity suggests that V445 Puppis probably contains a massive white dwarf accreting at high rate from a helium star companion making it part of a population of binary stars that potentially lead to supernova Ia explosions due to accumulation of helium-rich material on the surface of a massive white dwarf.

Subject headings: novae, cataclysmic variables — stars: individual (V445 Puppis)
— instrumentation: adaptive optics

1. Introduction

Accretion onto compact objects can lead to a range of explosive phenomena since their accreted layers can reach densities and temperatures high enough to initiate nuclear burning.

¹Center for Astrophysics, 60 Garden Street, Cambridge, MA 02138-1516

²School of Physics and Astronomy, Southampton University, Highfield, Southampton SO17 1BJ, United Kingdom

Helium novae are expected to occur during periods of high mass-accretion rates ($\dot{M} \sim 10^{-9} - 10^{-6} M_{\odot} \text{ yr}^{-1}$) of He-rich material through unstable helium burning via helium shell flashes (Iben & Tutukov 1991). In such events, typically $\sim 10^{-4} - 10^{-2} M_{\odot}$ of fuel is ignited on the surface of the accretor (Kato & Hachisu 1999; Yoon & Langer 2004; Bildsten et al. 2007). Models of the binaries that experience such helium novae generally consist of a $0.6 - 0.8 M_{\odot}$ CO white dwarf (the accretor) with a lower-mass H-deficient companion (the donor). The donor can be either a non-degenerate helium star (e.g., Yoon & Langer 2004) or a semi-/fully degenerate star. The latter are usually referred to as AM CVn systems, representing a class of ultra-compact helium-transferring binaries (Nelemans et al. 2004; Bildsten et al. 2007; Roelofs et al. 2007).

Some of these compact binaries may lead to sufficient mass accumulation onto the primary to be viable supernova Ia progenitors after successive He novae (Iben & Tutukov 1994; Kato et al. 1989; Yoon & Langer 2003; Tutukov & Fedorova 2007; Wang et al. 2009). Accreting massive white dwarfs in close binary systems are the favoured progenitors of supernova Ia explosions (Branch & Nomoto 2007; Parthasarathy 2007). Possible binary channels are typically divided into single-degenerate scenarios involving hydrogen-rich companions versus double-degenerate progenitors. The latter include the white dwarf plus He-star and double white dwarf pathways. To date, only about a dozen promising single-degenerate type Ia progenitors have been identified (see, e.g., Parthasarathy 2007). U Scorpii and RS Ophiuchi represent the two different classes of hydrogen-rich companion stars in the supernova Ia progenitors: main-sequence or slightly evolved stars, and red giants, respectively (Li & van den Heuvel 1997). Ongoing supernova searches are, however, revealing a growing diversity of type Ia explosion events, which challenge current formation scenarios. It could be that, despite their low predicted frequency, the helium star donor channel to type Ia explosion is successful in explaining some of the diversity observed, such as the population of young Ia progenitors (Mannucci et al. 2006; Wang et al. 2009).

V445 Puppis (Nova Puppis 2000) is the first, and so far only, helium nova detected (Ashok & Banerjee 2003; Kato & Hachisu 2003). The nova outburst of V445 Puppis was first noticed on 23 November 2000 (Kato et al. 2001), and the optical outburst characteristics are those of a slow nova. Optical (Wagner et al. 2001; Iijima & Nakanishi 2008), near-infrared (Ashok & Banerjee 2003) and mid-infrared (Lynch et al. 2001) spectra of V445 Puppis obtained during outburst immediately revealed its most peculiar and defining characteristic: the complete absence of hydrogen in the ejecta.

The outburst light curve has been modelled (Kato & Hachisu 2003; Kato et al. 2008) by free-free emission and an optically thick wind, following a helium shell flash on the surface of an accreting massive white dwarf. A lower limit on the mass of the accreting white dwarf of

$M \geq 1.35 M_{\odot}$ is inferred by Kato et al. (2008), making V445 Puppis a possible progenitor of a supernova Ia from a helium-rich donor channel. In these models, the white dwarf is expected to grow in mass as the mass ejected through repeated helium nova outbursts is less than the accreted mass (Kato & Hachisu 1999).

V445 Puppis provides the first empirical benchmark for a helium-dominated outburst on the surface of a white dwarf. In Section 2 we present new observations of V445 Puppis taken 5 – 7 years after outburst, and determine the distinct evolution of the resolved nova shell from a spatio-kinematic analysis (Section 3). This leads to a robust distance determination to V445 Puppis. In Section 4, we discuss the implications of the distance derived here on the nature of the underlying binary.

2. Imaging and Spectroscopic Observations

We acquired high angular-resolution images of V445 Puppis in the near-infrared K_s band using the NAOS/CONICA adaptive optics (AO) system (Rousset et al. 2003; Lenzen et al. 2003) on the Very Large Telescope (VLT). For these observations, the S27 camera was used which has a scale of 27.15 milli-arcsec per pixel and a total field of $28'' \times 28''$. The images were taken on four epochs spread over a two-year period; details of the VLT observations are given in Table 1. The nearby ($24''$) and relatively bright ($V \sim 15.5$ mag) star GSC2.3 S3EQ038054 (Lasker et al. 2008) was selected as the AO reference star. The achieved FWHM on target after AO corrections ranges from $0.09''$ to $0.14''$. Separate observations of a pair of close stars – also separated by $24''$ and of similar brightness to GSC2.3 S3EQ038054 – were obtained for deconvolution purposes; the selected PSF star is GSC2.3 S3EQ038567 (Lasker et al. 2008). We deconvolved the images using the standard Richardson-Lucy technique (Richardson 1972; Lucy 1974; Karovska et al. 1997). It took from 5 to 20 iterations for the deconvolution to converge to a stable result.

In addition, integral field unit (IFU) spectroscopy was obtained with the IMACS spectrograph on the 6.5-m Magellan Baade telescope on 4 January 2006. In the f/4 camera mode that we employed, the IMACS IFU mode provides two fiber bundles covering $5'' \times 4.15''$ on the sky sampled with $0.2''$ per fiber element (Schmoll et al. 2004). Spectral coverage was $4465 - 7634 \text{ \AA}$ sampled at $0.38 \text{ \AA}/\text{pixel}$ across four $2k \times 4k$ CCD detectors using the 600 grating. We acquired seven 30-min exposures with V445 Puppis centered in one of the fiber bundles under $0.5''$ seeing conditions with clear skies. The second fiber bundle was used to measure simultaneously the sky $60''$ away from our target. In order to improve the spectral extraction and remove cosmic rays, the seven exposures were first median-combined in 2D. Fiber spectra were then extracted using a normal extraction procedure covering relevant

target and sky fibers. Target and sky spectra were wavelength calibrated using He-Ne-Ar lamp exposures, and then differenced to produce sky-subtracted 1D fiber spectra sampling the target bundle. On three occasions V band imaging was secured with IMACS. These images were calibrated using Landolt standards (Landolt 1992) and the derived magnitudes are plotted in Fig. 1.

Supplementary optical (3600 – 9000 Å) and near-infrared (15000 – 25000 Å) long-slit spectroscopy was obtained on 17 December 2003 and 6 October 2005. Details of the former are presented in Woudt & Steeghs (2005). The near-infrared spectroscopy was obtained in service mode on the 3.5-m New Technology Telescope using the SOFI spectrograph. The spectral coverage includes the H and K_s photometric bands, sampled at 10.2 Å/pixel.

We frequently monitored V445 Puppis at near-infrared wavelengths, from 2002 March to the present, using the Infrared Survey Facility and the SIRIUS camera (Nagayama et al. 2003) at the Sutherland station of the South African Astronomical Observatory; the latter allows simultaneous J , H and K_s imaging over a 7.7×7.7 arcmin field of view. The IRSF aperture-corrected photometry has been calibrated with photometry from the 2MASS Point Source Catalog (Skrutskie et al. 2006) using stars in the field of view. 2MASS magnitudes of these stars have been converted to the IRSF photometric system to determine proper zero points, after which the calibrated IRSF magnitudes of V445 Puppis have been converted back to the 2MASS system. The magnitudes of V445 Puppis in the 2MASS photometric system are given in Table 2.

3. Results

3.1. Brightness evolution

The long-term brightness evolution of V445 Puppis at optical and near-infrared wavelengths is shown in the lower panel of Fig. 1. It shows V445 Puppis before outburst in the V band and the 2MASS J , H and K_s single epoch (Skrutskie et al. 2006), during outburst in optical¹ and near-infrared (Ashok & Banerjee 2003), and post-outburst where the initial H and K_s observation after decline is from Ashok & Banerjee (2003) and the remainder of the post-outburst light curve is derived from our IRSF/SIRIUS J , H , K_s and Magellan/IMACS V band observations. The exact date of outburst is uncertain, but is constrained by a lower detection limit ($V < 12$ mag) of V445 Puppis less than two months prior to its discovery in

¹All optical pre-outburst and outburst observations are from VSNET, see Ashok & Banerjee (2003) for details.

outburst, see the discussion in Ashok & Banerjee (2003). The outburst has occurred within the two vertical dashed lines in Fig. 1. The four epochs of high-angular resolution imaging with NAOS/CONICA are indicated by the vertical dotted lines, the three epochs of IMACS observations are marked by solid vertical bars.

More than 8 years after outburst, V445 Puppis is still highly reddened and ~ 6 magnitudes below its pre-outburst brightness as measured in the J band and 5.2 magnitude below its pre-outburst brightness in the V band; at this phase, optical light is dominated by line emission with a negligible continuum contribution. In the last 2 – 3 years, V445 Puppis has steadily declined in brightness in the H and K_s bands, but stayed constant in the J band. Where the J band flux has almost no continuum component and is dominated by the $1.0830 \mu\text{m}$ HeI recombination line emission, the H and K_s bands contain a thermal continuum component of $T = 250 \text{ K}$ (Lynch et al. 2004). The latter band also contains the $2.0581 \mu\text{m}$ HeI recombination line which has an equivalent width of $\sim -180 \text{ \AA}$ as derived from our SOFI spectrum. The upper panel of Fig. 1 shows the $(J - H)^0$ and $(H - K_s)^0$ color evolution of V445 Puppis, where the photometry has been corrected for the Galactic foreground extinction of $E(B - V) = 0.51 \text{ mag}$ (Iijima & Nakanishi 2008). We refer to Sect. 4.1 for a more detailed discussion on the Galactic foreground extinction. The fading in the H and K_s band – at fairly constant $(H - K_s)^0$ color – could indicate a cooling of the thermal continuum component over the last 2 – 3 years. *Spitzer* observations of V445 Puppis taken during this phase (PI: Banerjee) will be able to constrain the temperature of the cool thermal component.

3.2. The expanding nova shell

Fig. 2 shows the deconvolved near-infrared K_s (false color) images obtained at the four different epochs. The deconvolved field of view of the March and December 2005 images is $1.66'' \times 1.52''$, whereas the October 2006 and March 2007 observations are displayed on a wider scale of $3.48'' \times 3.48''$. The incredible detail seen on these small scales – the ejecta only span $2'' - 3''$ on the sky – is possible thanks to the adaptive optics technology on large ground-based telescopes. This allows a clear morphological description and dynamical analysis of the evolving nova ejecta. In Fig. 3 we show the shell in March 2005 (in contours) superimposed on the March 2007 observations to demonstrate the distinct expansion of the shell.

The images unambiguously show a bipolar shell – initially with a very narrow waist – with lobes on each side (north-east: NE, and south-west: SW) of a centrally-obscured region covering the nova remnant. At all epochs, two knots are seen at either extreme end

of the nova shell. This shell is unlike any previously observed classical nova shell, though strongly reminiscent of bipolar planetary nebulae (PNe), protoplanetary nebulae (pPNe) (Balick & Frank 2002), and the symbiotic Mira nebula Hen 2-104 (Corradi et al. 2001). In the case of V445 Puppis though, the large expansion velocity of the shell is clearly consistent with a nova explosion, rather than a PN outflow. The central obscuration appears to be confined to a plane nearly perpendicular to the two lobes of the bipolar shell. Such an obscuration has also been seen in various pPNe (e.g. in Hen 401, Sahai et al. 1999) where it is interpreted as a thick circumstellar dust disk. As the ejecta of V445 Puppis had a dominant carbon signature shortly following the outburst, and as the nova remnant has now been obscured for the last 8 years following outburst, it is likely that this dust is largely concentrated in a plane perpendicular to the lobes where it continues to obscure the underlying binary. Given the large obscuration post-outburst (see lower panel Fig. 1), this dust disk must be a direct consequence of the November 2000 outburst.

3.3. Spatio-kinematic analysis

In Fig. 4 we show the spatially-resolved velocity profile of the He I 7065 Å line extracted from our IFU spectroscopy. These were observed close to the second epoch of the VLT NACO K_s band imaging campaign. We averaged together several fibers across the minor axis of the nova-shell to generate each plotted line profile, sampling the shell approximately along its major axis, from east to west on the sky. This sampling at 0.17'' per row of fibers is seeing-limited with a FWHM of 0.5'' during our observations. Two components are distinctly visible, associated with each side of the nova shell, as expected from a bipolar outflow (Solf & Ulrich 1985). Peak emission of the NE lobe is at -1270 km s^{-1} and $+1140 \text{ km s}^{-1}$, whereas peak emission of the SW lobe is at -760 km s^{-1} and $+1720 \text{ km s}^{-1}$; typical measurement errors are $\pm 20 \text{ km s}^{-1}$. The offset is presumably due to a mild inclination to the line-of-sight, which results in a different mean radial velocity for the two lobes (-60 km s^{-1} versus $+480 \text{ km s}^{-1}$ for the NE lobe and the SW lobe, respectively). The mean of these velocity components agrees well with the systemic radial velocity of V445 Puppis of $224 \pm 8 \text{ km s}^{-1}$, reported by Iijima & Nakanishi (2008). All the emission lines in the Magellan IFU spectra reveal the same velocity structure, see also the summed spectrum shown in Fig. 5. The He I 7065 Å was chosen since it is one of the strongest unblended lines and allows for a cleaner measurement compared to the strong but blended O features. Moreover, the overall structure of the emission lines (as deduced from a long-slit perspective) has not changed significantly over ~ 2 years (see right panel of Fig. 4) which suggests that the bulk outflow pattern has not evolved substantially.

Motivated by the observed kinematics, we model the velocity profile with a simple bipolar velocity field (non-variable in time) following the description in Solf & Ulrich (1985), namely:

$$v_{ex}(\phi) = v_e + (v_p - v_e) \sin^\alpha(|\phi|), \quad (1)$$

where ϕ is the latitude angle (the poles are at $|\phi| = 90^\circ$, the equator at $\phi = 0^\circ$), v_e is the equatorial velocity and v_p is the polar velocity. The exponent α controls the degree of bipolarity: large α implies strong bipolarity. In our models we kept v_e constant at 500 km s^{-1} based on the (equatorial) expansion velocity deduced from the P Cygni profile during outburst (Iijima & Nakanishi 2008). From the velocity profile alone (Fig. 4), no unique solution to the bipolar velocity field (read: α) exists, although each value of α gives a best fit value for the inclination i , v_e and v_p . A wide range of models ($\alpha = 6 - 14$) all indicate a bipolar shell which is closely aligned with the plane of the sky ($i_{\text{shell}} = 5.8^\circ - 3.7^\circ$, respectively), giving further support to the presence of an orthogonal dust structure closely aligned along the line of sight causing the observed extinction.

Measurements of the angular separation of peak emission perpendicular to the polar axis were obtained at $\Delta x = \pm 0.3''$, $\pm 0.6''$, and $\pm 0.8''$ (the latter only for the last two epochs) from the center, where x is the distance along the polar (major) axis (i.e. $\phi = \pm 90^\circ$); they are listed in Table 3 and shown in the left panel of Fig. 6. Typical errors on the positional measurements are $\pm 0.01''$ for the first two epochs and $\pm 0.02''$ for the latter two epochs. Models with $\alpha < 10$ are excluded from the high-resolution imaging (too round). Similarly, models with $\alpha > 14$ are excluded as they would have resulted in such high elongation of the shell that it should have been visible at $\Delta x = \pm 0.8''$ at the first epoch. This was not observed.

From the combined spatio-kinematic observations and models, a distance to the nova shell can be obtained; x and y values from the models have been derived from equations 3 and 4 from Solf & Ulrich (1985) and differences with the observed values minimised by varying the distance to the nova. Even though we are comparing the velocity field of *optical* emission lines with the *near-infrared* K_s band images of V445 Puppis, it should be noted that the velocity structure of the optical and near-infrared recombination lines of He I are identical (see right panel of Fig. 4); we are therefore probing the same outflow component at optical and near-infrared wavelengths. The distance thus derived is relatively insensitive to the choice of α ; acceptable model fits ($\alpha = 10 - 14$) lead to distances in the range of $7.8 - 8.4$ kpc. These values are consistent with the lower limit of 6 kpc deduced from the presence of interstellar Na D absorption lines at $v_{\text{lsr}} = +73.5 \text{ km/s}$ (see, Brand & Blitz 1993) in the high-resolution spectrum of V445 Puppis during outburst (Iijima & Nakanishi 2008).

We superimpose the best fit model ($\alpha = 12$) on the measurements in the left panel of Fig. 6. The parameters of the $\alpha = 12$ model are given in Table 4 where the formal measurement error is given as well as the systematic error for different allowed values of α . The expected radial velocity profile from the $\alpha = 12$ model – along the major axis of the shell – is shown in the lower right of Fig. 6 and can be compared with the observed profile shown in Fig. 4. The bulk velocities ($v_p = 6720 \pm 650 \text{ km s}^{-1}$) are on the high end compared to hydrogen-rich novae, though not unreasonable, see for example RS Oph with $v_p = 5600 \pm 1100 \text{ km s}^{-1}$ (Bode et al. 2007). We thus derive a distance to V445 Puppis of $8.2 \pm 0.5 \text{ kpc}$ (including systematic errors) by combining our dynamical study of the emission lines from the shell with on-sky expansion rates measured in AO images.

It is of interest to note that the knots behave independently from the shell. Their apparent linear expansion on the sky ($0.217'' \pm 0.010'' \text{ yr}^{-1}$), shown in the upper right panel of Fig. 6, results in a deprojected polar velocity at 8.2 kpc of $\sim 8450 \text{ km s}^{-1}$, larger than the 6720 km s^{-1} derived from the bipolar velocity field of the shell. Moreover, a simple extrapolation of the expanding knots back to the center of the nova remnant coincides closely in time with a strong radio flare observed at $\sim \text{HJD } 2452185$ (Rupen et al. 2001). This suggests the knots originate from a ~ 345 -d delayed post-outburst outflow rather than the nuclear burning event itself. The bipolar shell on the other hand is consistent with uniform expansion since the start of the nova outburst.

Detailed 1-D hydrodynamical models following the evolution of PNe (Schönberner et al. 2005; Mellema 2004) indicate that in the interstellar wind model of PNe the measured edges of the PN shells are due to either ionisation or shock fronts, which move at different velocities from those measured with spectroscopy; in such case the expansion parallax always gives a lower limit to the true distance. This was indeed observed in the symbiotic star Hen 2-147 (Santander-García et al. 2007), where the distance derived from the expansion parallax is a factor of 2 lower than the distance determined from the period-luminosity relation for its Mira star component. Santander-García et al. (2007) argue for the presence of a shock front in the case of Hen 2-147. In the case of V445 Puppis, it is less clear that the edges in Fig. 2 arise from a strong shock front. Our optical spectra show a distinct lack of lines related to shock ionisation, e.g. both [NII] and [SII] 6717/6731 Å are absent, as seen in Fig. 5.

A direct comparison with the Schönberner et al. (2005) models is not appropriate given the order of magnitude difference in outflow velocities. We do not - a priori - expect a large distance correction factor for V445 Puppis. The deprojected velocities of the polar blobs are already on the high end of speeds observed in nova ejecta; a significantly greater distance would imply velocities more typical of supernovae rather than classical novae. Moreover, the absence of strong shock lines, the consistency of the HeI recombination line profiles

(kinematic analysis), linked with the dominance of the HeI recombination line in the K_s passband (spatio analysis) suggests that the outflow velocity matches the angular expansion closely. Nonetheless, to estimate by what amount the expansion parallax could underestimate the true distance in V445 Puppis detailed (magneto)hydrodynamic simulations (see, e.g., Dennis et al. 2009) with realistic input parameters as identified here – and the possible presence of pre-existing circumstellar material – must be obtained.

4. Discussion

4.1. Pre-outburst conditions

With the distance known, the nature of the helium nova progenitor can be constrained from pre-outburst observations. Unfortunately, not much is known of V445 Puppis prior to outburst. Apart from optical ($V = 14.5$ mag, from VSNET, see Ashok & Banerjee (2003)) and near-infrared (2MASS: $K_s = 11.52$ mag) flux measurements (see lower panel of Fig. 1), neither spectrum nor orbital period have been obtained prior to outburst. We verified the plate archives at the Harvard-Smithsonian Center for Astrophysics for prior outbursts (or sustained long periods of obscuration indicative of a missed outburst). Despite good time coverage and the fact that V445 Puppis could be identified on many plates at approximately constant brightness (based on visual comparison with nearby stars in the field), we could find no signatures of a previous outburst in the 1897 – 1955 time frame.

V445 Puppis is located at the low Galactic latitude of $b = -2.19^\circ$, which at a distance of 8.2 ± 0.5 kpc translates to a height below the Galactic Plane of 313 ± 19 pc. At that distance, and that far below the Galactic Plane, one can use the IRAS/DIRBE Galactic reddening maps (Schlegel et al. 1998) to gauge the Galactic reddening towards V445 Puppis. In Fig. 7 we show the ratio of the measured reddening (at a given distance) to the total line-of-sight Galactic reddening for open clusters in the Milky Way (Kharchenko et al. 2005) in the Galactic latitude range $1^\circ \leq |b| \leq 4^\circ$ and for $E(B - V)_{\text{Schlegel}} \leq 2.5$, as a function of height above/below the Plane and distance, respectively. The reddening maps of Schlegel et al. (1998) are not well-calibrated at low Galactic latitude; from colors of galaxies discovered at low Galactic latitude behind the southern Milky Way it appears that the reddening values from Schlegel et al. are too high (Schröder et al. 2007) and that the true value is 87% of the Schlegel et al. (1998) reddening, e.g. $E(B - V)_{\text{Schlegel}}^{\text{cal}} = 0.87E(B - V)_{\text{Schlegel}}$.

Comparing the location of V445 Puppis to open clusters within 10 degrees of V445 Puppis (big filled circles in Fig. 7), we deduce that Galactic foreground reddening towards V445 Puppis is probably in the range of $E(B - V) = 0.51 - 0.68 = 0.75 - 1.0 E(B - V)_{\text{Schlegel}}^{\text{cal}}$,

as marked by the arrow in Fig. 7. The lower limit given here could be a conservative one due to a selection effect; given the relative poor angular resolution of the reddening maps, the open clusters which set the lower ratio limits (those observed at large distances and large height above/below the Galactic plane) are likely to be observed through small-scale patches of relatively lower extinction compared to their surrounding. Finally, taking the equivalent widths of the two interstellar Na D components (Iijima & Nakanishi 2008), a value of $E(B - V) = 0.62$ is inferred using the calibration of Munari & Zwitter (1997). This value falls within our deduced limits.

Taking the lower limit of the Galactic reddening towards V445 Puppis ($E(B - V) = 0.51$), we derive a pre-outburst color of V445 Puppis of $(V - K)^0 = 1.58$ mag, assuming a standard Galactic extinction law (Cardelli et al. 1989). This is significantly redder than the likely binary progenitors – high \dot{M} AM CVn systems or systems with helium stars donors – which typically have $(V - K)^0 \approx -0.6$. A red giant donor (sympiotic nova) can be excluded on the basis of the pre-outburst colors.

This suggests the presence of substantial circumstellar (CS) reddening before the November 2000 outburst, which is not unreasonable given the possibility of previous outbursts or material expelled during a common envelope phase. The CS reddening around V445 Puppis does not necessarily have to follow a standard Galactic extinction given the current carbon-rich ejecta; Bergeat et al. (1999) find some deviations from a standard reddening law for CS reddening around a number of carbon-rich R CrB stars. In the right panel of Fig. 4, we compare the line profile of the 7065 Å and 2.0581 μm He I recombination lines, obtained close in time and both normalised by peak blueshifted emission. As expected, the redshifted component of the optical line (at +1140 km s⁻¹) appears dimmer compared to its near-infrared counterpart, due to dust obscuration within the shell. For a standard Galactic reddening law (Cardelli et al. 1989), we expect a ratio of peak emission of near-infrared (2.0581 μm) to optical (7065 Å) of 7. The ratio observed in V445 Puppis is 3.4, substantially less and indicative of a low ratio of total-to-selective extinction, $R_V \approx 2.5$ (Fitzpatrick 1999). The shell of V445 Puppis offers an opportunity to determine the nature of the dust extinction in carbon-rich outflows. The new X-shooter instrument on the VLT will be ideal to obtain simultaneous optical to near-infrared medium-to-high resolution spectroscopy of both NE and SW shells.

To make the pre-outburst color of V445 Puppis consistent with the intrinsic colors of likely progenitor binaries, a (maximum) additional color excess of $A_V - A_K = 2.2$ mag requires $A_V = 2.5$ mag for $R_V = 3.1$ (standard reddening law), or $A_V = 2.8$ mag for $R_V = 2.5$. The uncertainty in A_V introduced by the different reddening laws, however, is small compared to the uncertainty in the bolometric correction needed to arrive at the pre-outburst luminosity

of V445 Puppis.

We thus determine a pre-outburst extinction-corrected brightness of at least $V^0 = 12.9$ mag (corrected for Galactic reddening only), but more likely $V^0 \approx 10.1 - 10.4$ mag (including circumstellar reddening correction), with the range in the latter allowing for differences in the CS reddening law. The corresponding absolute magnitudes are $M_V^0 = -1.7$ and -4.2 to -4.5 mag, respectively. For a range of likely bolometric corrections ($BC = -1$ to -2.5 , Roelofs et al. (2007); Heber & Schoenberner (1981)), the pre-outburst luminosity of V445 Puppis is $\log L/L_\odot = 3.3 \pm 0.3$ (corrected for Galactic extinction only), or $\log L/L_\odot = 4.34 \pm 0.36$ (including circumstellar reddening correction).

It has not escaped our attention that hydrogen-deficient carbon (HDC) stars also occupy this luminosity regime. With a larger distance – this paper – and a larger Galactic reddening correction (Iijima & Nakanishi 2008), the possibility that V445 Puppis belongs to the class of HDC stars can no longer be rejected on luminosity grounds, cf. Ashok & Banerjee (2003). The (Galactic) extinction-corrected $(V - K_S)^0$ colors of V445 Puppis are not too dissimilar from the HDC star HD 182040 (Brunner et al. 1998). It is not clear, though, what can cause a luminosity increase of 6 magnitudes and a rapidly expanding shell from a HDC star; the overall light curve appears much better described by an event near a compact, massive white dwarf.

4.2. Shaping of the nebula

Deviations from the simple outflow model presented in Section 3 could provide clues to the mechanism responsible for shaping the nebula. Although the dynamical model fits the shell remarkably well, the largest deviations occur nearest to the nova remnant at the earliest epochs. The nebula initially had a very narrow waist, followed by a rapid broadening of the waist close to the nova remnant.

To produce very narrow waists in PNe, collimated fast winds (CFW) are needed in systems with high density gas in an equatorial plane close to the source of the CFW (Soker & Rappaport 2000). It is unclear what collimated the fast wind in V445 Puppis. At the moment it seems likely that an equatorial disk/torus already existed pre-outburst, given the large pre-outburst circumstellar reddening deduced in Section 4.1. Once the present optically-thick dust disk clears (Fig. 2 – presumably additional material was ejected in the equatorial plane during the November 2000 outburst) and a relatively unobscured view of the nova remnant is possible, alternative origins of the collimated outflow could be investigated, e.g. the presence of a rapidly rotating magnetic white dwarf.

The shell of V445 Puppis is unique for a classical nova. Although many novae show bipolar shells, for example the classical nova HR Del (Harman & O’Brien 2003) and recurrent nova RS Oph (Bode et al. 2007; Sokoloski et al. 2008), the shell in V445 Puppis reflects the most collimated outflow seen in any nova. The knots are moving at jet-like velocities of $\gtrsim 8000 \text{ km s}^{-1}$. They can be a consequence of a jet-activity about 350 days after the main outburst which is not long after the sudden drop off in the V band is seen (Ashok & Banerjee 2003) and coincides with the radio flare (Rupen et al. 2001). In the symbiotic nova CH Cygni, a drop in V band magnitude is associated with the onset of a radio jet ejection, see e.g. Karovska et al. (2007).

4.3. V445 Puppis as a proto-type helium nova

At a distance of 8.2 kpc, the maximum brightness at outburst ($V = 8.6 \text{ mag}$) is consistent with the Eddington luminosity of a massive white dwarf. Moreover, the pre-outburst luminosity of V445 Puppis of $\log L/L_{\odot} = 4.34 \pm 0.36$ appears to rule out an AM CVn progenitor and may require both a luminous accretion flow as well as a bright donor. For comparison, a $1.3\text{-}M_{\odot}$ white dwarf accreting at $\dot{M} \sim 10^{-6} M_{\odot} \text{ yr}^{-1}$ would give an expected accretion luminosity of $\log L/L_{\odot} = 3.7$. Similarly, the luminosity of a moderately massive, evolved helium star is around $\log L/L_{\odot} \approx 3.7$ (Yoon & Langer 2003).

With the distance determined in this paper, a revised mass of the dust shell of $1.5 \times 10^{-5} M_{\odot}$ is derived following Lynch et al. (2004). This is consistent with Kato & Hachisu (2003), but we note that the mass depends strongly on the assumed temperature of the shell and will ultimately be best constrained by mid- to far-infrared data of V445 Puppis recently obtained by *Spitzer*. This mass is likely to be a lower limit given the large optical depth of the equatorial dust disk.

The various components of V445 Puppis (the dust disk, the bipolar shell) clearly show that the immediate environment of V445 Puppis is sculpted either directly or indirectly by (repeated) outbursts. If V445 Puppis is representative of its class (of helium novae), the helium counterparts to the classical hydrogen-rich novae result in more substantial circumbinary reddening due to the carbon-rich outflow.

Validation of the white dwarf + helium star model as the appropriate binary configuration of V445 Puppis will come from the determination of its orbital period. Unfortunately, this can only be done once the optically thick dust disk surrounding the nova remnant becomes transparent. Given the low inclination of the bipolar outflow, the implied inclination of the equatorial plane which corresponds to the orbital plane of the binary is $\sim 86^{\circ}$. We thus

expect this to be an eclipsing binary, which would further facilitate our ability to constrain the component masses.

4.4. V445 Puppis as a candidate Ia progenitor

There are several indirect suggestions that the white dwarf in V445 Puppis is massive: the maximum luminosity during outburst, the large velocities of the ejected blobs, and its pre-outburst (accretion) luminosity.

The lack of strong soft X-ray emission pre-outburst, as is expected from a supersoft source (Yoon & Langer 2003) could be explained by the substantial interstellar and circumstellar absorption which currently totally obscures the underlying accreting binary. V445 Puppis has not been detected in the ROSAT all-sky survey.

Our derived luminosity is consistent with the massive white dwarf + helium star model of Yoon & Langer (2003), but see also Kato et al. (2008). It is likely that V445 Puppis belongs to a class of binaries that, in principle, could lead towards supernovae of type Ia. Given that the expected lifetime of a massive white dwarf + helium star binary is short, these progenitors are associated with the relatively young ($\sim 10^8$ yr) population of Ia SNe.

Whether V445 Puppis itself eventually leads to a supernova Ia event, or if the current helium nova has pre-empted that pathway, depends critically on the mass accumulation efficiency on the surface of the white dwarf and the mass ejected during this nova outburst. This remains a topic of debate.

We kindly acknowledge Tetsuya Nagata for scheduling the IRSF observations of V445 Puppis and thank all the service observers for their observations. The VLT observation of V445 Puppis was also performed in service mode and we kindly thank the service observers for their efforts in obtaining these data. PAW and BW acknowledge the National Research Foundation and the University of Cape Town for financial support. DS acknowledges Smithsonian Astrophysical Observatory Clay fellowship and a STFC Advanced Fellowship. MK is a member of the Chandra X-ray Center, which is operated by the Smithsonian Astrophysical Observatory under NASA Contract NAS8-03060. We thank the Harvard College Observatory plate curator for access to the plate stacks. We thank the referee for the useful comments given.

Facilities: VLT (NAOS/CONICA): ESO Program number 075.D-0425.A/B, 078.D-0666.A/B, IRSF (SIRIUS), Magellan (IMACS-IFU).

REFERENCES

- Ashok, N.M., & Banerjee, D.P.K. 2004, *A&A*, 409, 1007
- Balick, B., & Frank, A. 2002, *ARA&A*, 40, 439
- Bergeat, J., Knapik, A., & Rutily, B. 1999, *A&A*, 342, 773
- Bildsten, L., Shen, K.J., Weinberg, N.N., & Nelemans, G. 2007, *ApJ*, 662, L95
- Bode, M.F., Harman, D.J., O'Brien, T.J., Bond, H.E., Starrfield, S., Darnley, M.J., Evans, A., & Eyres, S.P.S. 2007, *ApJ*, 665, L63
- Branco, D., & Nomoto, K.-I. 2007, *Nature*, 447, 393
- Brand, J., & Blitz, L. 1993, *A&A*, 275, 67
- Brunner, A.R., Clayton, G.C., & Ayres, T.R., *PASP*, 110, 1412
- Cardelli, J.A., Clayton, G.C., & Mathis, J.S., 1989, *ApJ*, 345, 245
- Corradi, R.L.M., Livio, M., Balick, B., Munari, U., & Schwarz, H.E. 2001, *ApJ*, 553, 211
- Dennis, T.J., Frank, A., Blackman, E.G., DeMarco, O., & Balick, B. 2009, arXiv:0909.1100
- Fitzpatrick, E.L. 1999, *PASP*, 111, 63
- Harman, D.J., & O'Brien, T.J. 2003, *MNRAS*, 344, 1219
- Heber, U., & Schönberner, D. 1981, *A&A*, 102, 73
- Iben, I. Jr., & Tutukov, A.V. 1991, *ApJ*, 370, 615
- Iben, I. Jr., & Tutukov, A.V. 1994, *ApJ*, 431, 264
- Iijima, T., & Nakanishi, H. 2008, *A&A*, 482, 865
- Karovska, M., Carilli, C.L., Raymond, J.C., & Mattei, J.A. 2007, *ApJ*, 661, 1048
- Karovska, M., Hack, W., Raymond, J., & Guinan, E. 1997, *ApJ*, 482, L175
- Kato, M., & Hachisu, I. 1999, *ApJ*, 513, L41
- Kato, M., & Hachisu, I. 2003, *ApJ*, 598, L107
- Kato, M., Saio, H., & Hachisu, I. 1989, *ApJ*, 340, 509

- Kato, M., Hachisu, I., Kiyota, S., & Saio, H. 2008, *ApJ*, 684, 1366
- Kato, T., Kanatsu, K., Takamizawa, K., Takao, A., & Stubbings, R. 2001, *IAUC*, 7552
- Kharchenko, N.V., Piskunov, A.E., Röser, S., Schilbach, E., & Scholz, R.-D., 2005, *A&A*, 438, 1163
- Landolt, A.U. 1992, *AJ*, 104, 340
- Lasker, B.M., et al. 2008, *AJ*, 136, 735
- Lenzen, R., et al. 2003, *Proc. SPIE*, 4841, 944
- Li, X.-D., & van den Heuvel, E.P.J. 1997, *A&A*, 322, L9
- Lucy, L.B. 1974, *AJ*, 79, 745
- Lynch, D.K., Russel, R.W., & Sitko, M.L. 2001, *AJ*, 122, 3313
- Lynch, D.K., Rudy, R.J., Mazuk, S., Venturini, C.C., Puetter, R.C., & Perry, R.B. 2004, *AJ*, 128, 2962
- Mannucci, F., Della Valle, M., & Panagia, N. 2006, *MNRAS*, 370, 773
- Mellema, G. 2004, *A&A*, 416, 623
- Munari, U., & Zwitter, U. 1997, *A&A*, 318, 269
- Nagayama, T., et al. 2003, *Proc. SPIE*, 4841, 459
- Nelemans, G., Yungelson, L.R., & Portegies Zwart, S.F. 2004, *MNRAS*, 349, 181
- Parthasarathy, M., Branch, D., Jeffery, D. J., & Baron, E. 2007, *NewAR*, 51, 524
- Richardson, W. H. 1972, *JOSA*, 62, 55
- Roelofs, G.H.A., Groot, P.J., Benedict, G.F., McArthur, B.E., Steeghs, D., Morales-Rueda, L., Marsh T.R., & Nelemans, G. 2007, *ApJ*, 666, 1174
- Rousset, G., et al. 2003, *Proc. SPIE*, 4839, 140
- Rupen, M.P., Mioduszewski, A.J., & Dhawan, V. 2001, *IAUC*, 7728
- Sahai, R., Bujarrabal, V., & Zijlstra, A. 1999, *ApJ*, 518, L115

- Santander-García, M., Corradi R.L.M., Whitelock, P.A., Munari, U., Mampaso, A., Marang, F., Boffi, F., & Livio, M. 2007, *A&A*, 465, 481
- Schlegel, D.J., Finkbeiner, D.P., & Davis, M. 1998, *ApJ*, 500, 525
- Schmoll, J., Dodsworth, G.N., Content, R., & Allington-Smith, J.R. 2004, *Proc. SPIE*, 5492, 624
- Schönberner, D., Jacob, R., & Steffen, M. 2005, *A&A*, 441, 573
- Schröder, A.C., Mamon, G.A., Kraan-Korteweg, R.C., & Woudt, P.A. 2007, *A&A*, 466, 481
- Skrutskie, M.F., et al. 2006, *AJ*, 131, 1163
- Soker, N., & Rappaport, S. 2000, *ApJ*, 538, 241
- Sokoloski, J.L., Rupen, M.P., & Mioduszewski, A.J. 2008, *ApJ*, 685, L137
- Solf, J., & Ulrich, H. 1985, *A&A*, 148, 274
- Tutukov, A.V., & Fedorova, A.V. 2007, *ARep*, 51, 291
- Wagner, R.M., Foltz, C.B., & Starrfield, S.G. 2001, *IAUC*, 7556
- Wang, B., Meng, X., Chen, X., & Han, Z. 2009, *MNRAS*, 395, 847
- Woudt, P.A., & Steeghs, D.T.H. 2005, *Proc. AIP*, 797, 647
- Yoon, S.-C., & Langer, N. 2003, *A&A*, 412, L53
- Yoon, S.-C., & Langer, N. 2004, *A&A*, 419, 645

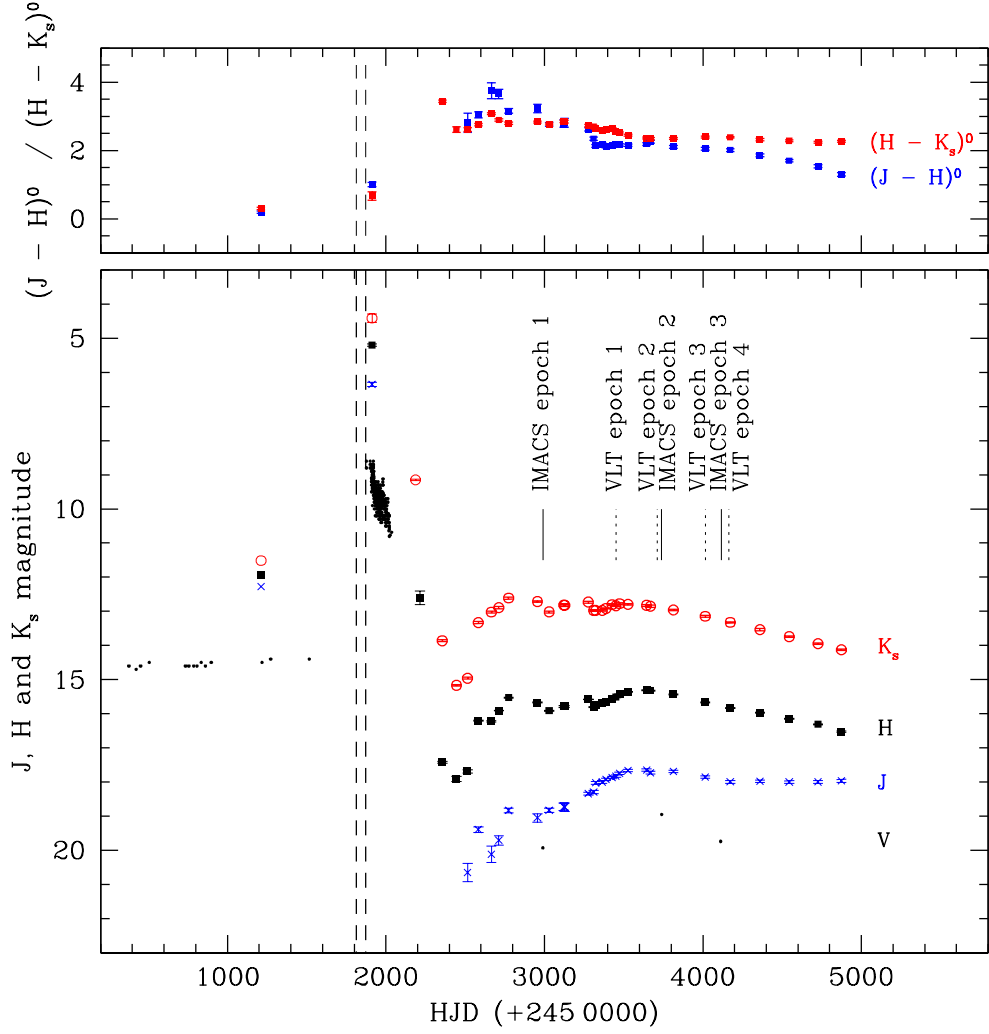


Fig. 1.— The optical and near-infrared light curve of V445 Puppis before, during and after outburst (lower panel). The exact date of outburst is uncertain, but constrained by the two vertical dashed lines. The times of VLT observations (Fig. 2) are indicated by the vertical dotted lines, times of Magellan/IMACS observations are indicated by the vertical solid lines. The top panel shows the near-infrared color evolution of V445 Puppis which is corrected for Galactic foreground extinction.

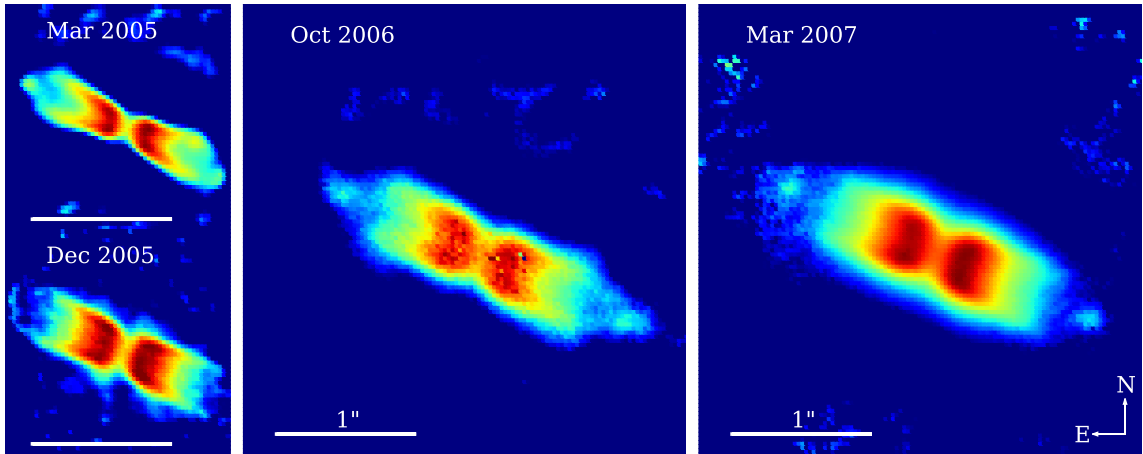


Fig. 2.— The evolving nova shell of V445 Puppis over a period of 2 years, obtained on four different epochs with NAOS/CONICA on the Very Large Telescope. All images are plotted on the same scale in the conventional North-East configuration with a sampling of 27.15 mas/pixel. The horizontal bar denotes a length of 1".

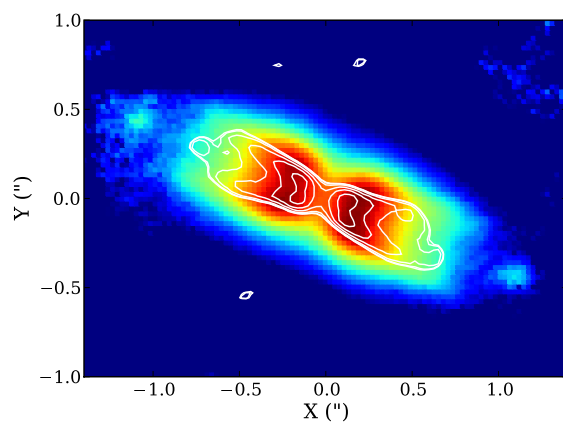


Fig. 3.— Two epochs of NAOS/CONICA imaging (March 2005 and March 2007) superimposed on top of each other (March 2005: contours, March 2007: false colour), revealing the distinct evolution of the shell. A spatial scale in arcseconds is provided on the both coordinate axes. North is up and East is to the left.

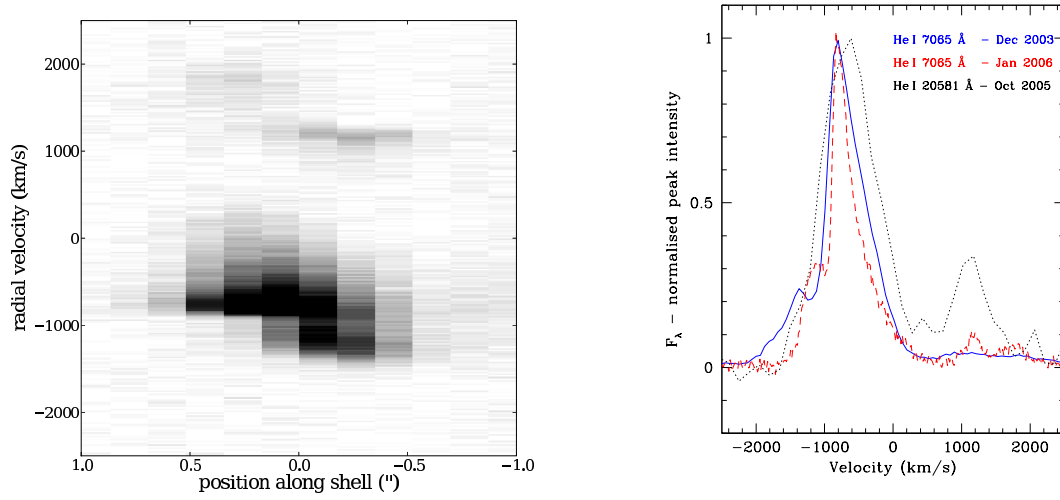


Fig. 4.— The spatially-resolved velocity structure of the He I 7065 Å line along the major axis of the nova shell running from East to West taken in January 2006 (left panel). The right panel shows the long-slit line profile of He I recombination lines in the optical (7065 Å) and near-infrared (2.0581 μm) over a 2-year time period.

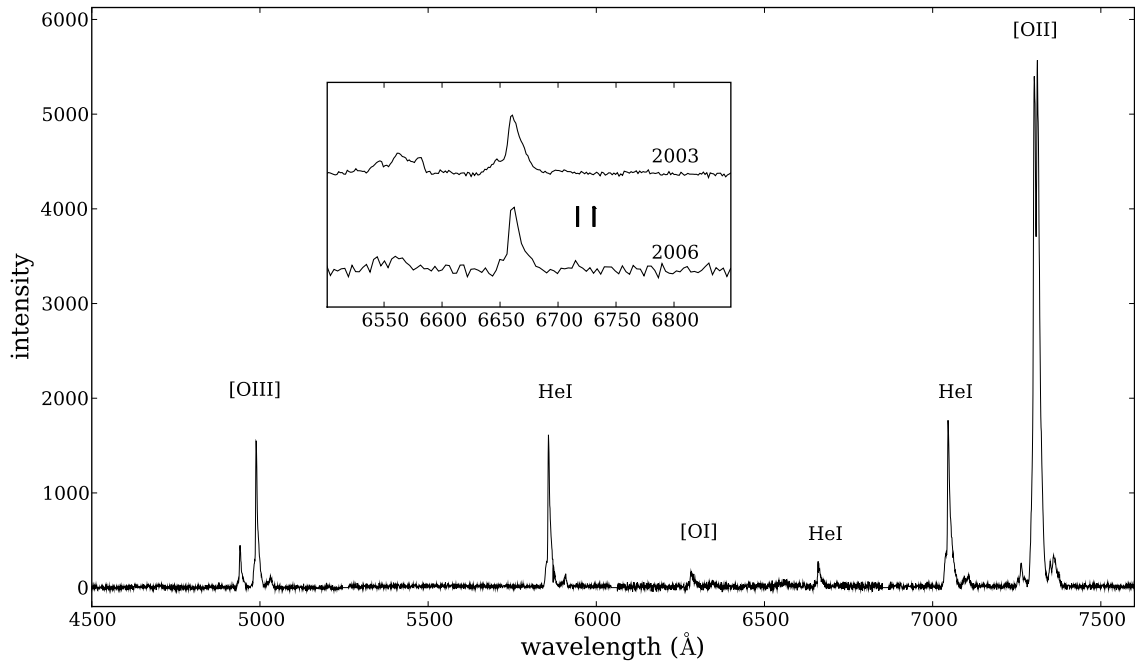


Fig. 5.— Average spectrum of V445 Puppis obtained in January 2006 by summing the IFU fibers containing the south-western lobe. Prominent lines are marked, including the He I 7065 Å line used for our kinematic analysis. The inset highlights the lack of the [S II] lines at 6717/6731 Å (marked by the vertical bars) that would be the signature of shock emission. For comparison, our (deeper) December 2003 spectrum (Woudt & Steeghs 2005) is also shown, further confirming the absence of [S II]. Note that the 2006 spectrum in the inset has been binned to 3.1 Å/pixel to improve the signal-to-noise and facilitate the comparison with the 2003 observations.

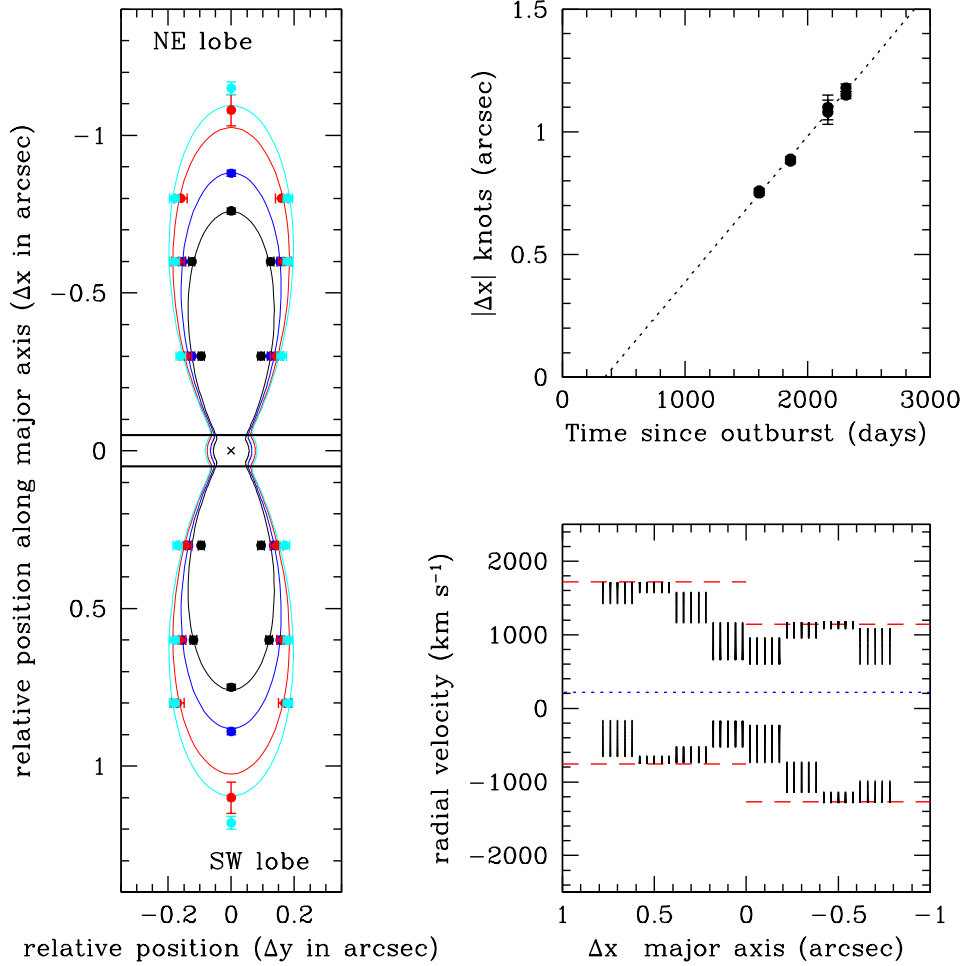


Fig. 6.— Left panel: Measured positions of peak emission of the nova shell at selected distances along the major axis, including the knots at the extremes of the shell (black: March 2005, blue: December 2005, red: October 2006, cyan: March 2007). The $\alpha = 12$ model (Table 4) spatio-kinematic model is overplotted (solid lines, colors as before). The top-right panel shows the change in position of the knots as a function of time. The lower-right panel displays the expected velocity profile of the shell along the major axis as derived from our best fit dynamical model (Table 4). The horizontal dashed lines are the measured peak velocities from Fig. 2.

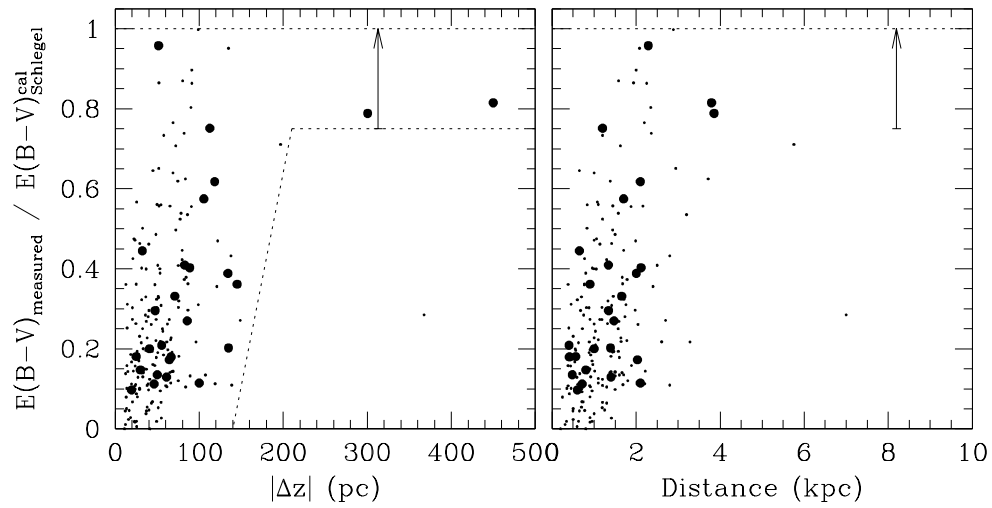


Fig. 7.— The ratio of measured reddening to the total line-of-sight reddening for Galactic open clusters (Kharchenko et al. 2005) as a function of height above/below the Galactic Plane (left panel) and distance (right panel). Only open clusters located at $1^\circ \leq |b| \leq 4^\circ$ and with $E(B-V)_{\text{Schlegel}}$ are shown. The total line-of-sight reddening has been reduced to 87% of the Schlegel et al. (1998) values as recalibrated by galaxies seen through the southern Milky Way (Schröder et al. 2007). The big filled dots represent open clusters within 10 degrees of V445 Puppis; the probable range of $E(B-V)$ for V445 Puppis is indicated by the arrow.

Table 1: Observing log of the NAOS/CONICA observations

Epoch	Date	MJD (start)	FWHM _{AO} (")	t_{int} (= N × NDIT × DIT) (s)
1	26 March 2005	245 3455.066	0.10	825 (= 5 × 11 × 15)
2	07 December 2005	245 3711.278	0.10	600 (= 10 × 1 × 60)
3	06 October 2006	245 4014.356	0.14	1620 (= 9 × 4 × 45)
4	03 March 2007	245 4162.015	0.09	1620 (= 9 × 4 × 45)

Table 2: Observing log of the IRSF/SIRIUS observations

Date	HJD (start)	t_{int} (s)	FWHM ($''$)	J (mag)	H (mag)	K_s (mag)
22 March 2002	245 2356.266	1000	0.97	–	17.419 ± 0.025	13.859 ± 0.027
19 June 2002	245 2445.185	600	1.31	–	17.907 ± 0.078	15.168 ± 0.025
28 August 2002	245 2515.657	900	1.38	20.650 ± 0.272	17.691 ± 0.045	14.957 ± 0.027
04 November 2002	245 2583.610	900	1.10	19.394 ± 0.084	16.205 ± 0.016	13.327 ± 0.030
25 January 2003	245 2665.326	900	1.51	20.116 ± 0.235	16.223 ± 0.016	13.021 ± 0.022
13 March 2003	245 2712.289	900	1.47	19.709 ± 0.136	15.907 ± 0.011	12.891 ± 0.031
14 May 2003	245 2774.242	900	1.08	18.834 ± 0.067	15.529 ± 0.014	12.611 ± 0.033
12 November 2003	245 2956.479	1200	2.02	19.052 ± 0.123	15.672 ± 0.015	12.715 ± 0.023
25 January 2004	245 3030.336	1200	1.80	18.825 ± 0.060	15.914 ± 0.010	13.017 ± 0.026
26 April 2004	245 3122.228	900	1.38	18.724 ± 0.103	15.788 ± 0.026	12.816 ± 0.025
02 May 2004	245 3128.205	900	1.76	18.740 ± 0.126	15.786 ± 0.027	12.822 ± 0.034
29 September 2004	245 3277.643	900	1.16	18.341 ± 0.046	15.580 ± 0.010	12.730 ± 0.028
31 October 2004	245 3310.582	900	1.87	18.291 ± 0.050	15.800 ± 0.013	12.973 ± 0.025
14 November 2004	245 3324.443	900	1.13	18.024 ± 0.039	15.745 ± 0.013	12.976 ± 0.016
25 December 2004	245 3365.395	1200	1.37	18.001 ± 0.041	15.675 ± 0.009	12.974 ± 0.025
17 January 2005	245 3388.458	900	1.37	17.923 ± 0.036	15.656 ± 0.008	12.914 ± 0.018
25 February 2005	245 3426.799	900	1.14	17.870 ± 0.034	15.569 ± 0.011	12.804 ± 0.026
22 March 2005	245 3451.865	900	1.10	17.829 ± 0.036	15.516 ± 0.009	12.837 ± 0.019
14 April 2005	245 3473.789	1200	1.14	17.742 ± 0.031	15.432 ± 0.007	12.775 ± 0.021
06 June 2005	245 3527.679	900	1.13	17.659 ± 0.035	15.361 ± 0.007	12.796 ± 0.026
30 September 2005	245 3644.622	900	1.17	17.648 ± 0.035	15.312 ± 0.012	12.826 ± 0.027
25 October 2005	245 3669.579	900	1.98	17.731 ± 0.040	15.323 ± 0.014	12.850 ± 0.031
20 March 2006	245 3814.745	900	1.19	17.686 ± 0.037	15.432 ± 0.011	12.959 ± 0.022
06 October 2006	245 4015.117	900	1.39	17.860 ± 0.034	15.662 ± 0.013	13.145 ± 0.024
13 March 2007	245 4172.804	900	1.42	17.995 ± 0.039	15.835 ± 0.010	13.323 ± 0.020
16 September 2007	245 4360.152	900	0.98	17.981 ± 0.036	15.975 ± 0.014	13.535 ± 0.030
19 March 2008	245 4544.781	900	1.16	18.000 ± 0.036	16.150 ± 0.011	13.745 ± 0.022
17 September 2008	245 4727.150	900	1.44	17.998 ± 0.041	16.311 ± 0.018	13.948 ± 0.023
11 February 2009	245 4873.778	900	2.03	17.969 ± 0.045	16.525 ± 0.020	14.128 ± 0.018

Table 3: Dimensions of the nova shell of V445 Puppis

Epoch	Δy at $ x = 0.3''$		Δy at $ x = 0.6''$		Δy at $ x = 0.8''$		Δx knots		errors
	(")	(")	(")	(")	(")	(")	(")	(")	(")
	NE	SW	NE	SW	NE	SW	NE	SW	
1	0.19	0.19	0.25	0.24	–	–	0.76	0.75	0.01
2	0.25	0.27	0.31	0.31	–	–	0.88	0.89	0.01
3	0.29	0.29	0.34	0.33	0.32	0.34	1.08*	1.10*	0.02
4	0.32	0.34	0.36	0.36	0.36	0.36	1.15	1.18	0.02

* The uncertainties in the positions of the knots at this epoch are $\pm 0.05''$.

Table 4: Bipolar outflow model and properties of V445 Puppis

PA shell	66 deg
α	12 $^{+2}_{-2}$
i_{shell}	3.9 $^{+0.2}_{+0.5} \pm 0.4$ deg
v_e	500 km s ⁻¹
v_p	6720 $^{+540}_{-600} \pm 250$ km s ⁻¹
v_{knots}	8450 $^{+210}_{-410} \pm 390$ km s ⁻¹
d	8.2 $^{+0.2}_{-0.4} \pm 0.3$ kpc